Nuclear Physics A536 (1992) 349–365
North-Holland

NUCLEAR
PHYSICS A

PROTON AND NEUTRON SUPERFLUIDITY IN NEUTRON STAR MATTER

M. BALDO[1], J. CUGNON[2], A. LEJEUNE[2] and U. LOMBARDO[1]

[1] *Dipartimento di Fisica, Univ. di Catania and INFN Sezione di Catania, Corso Italia, 57, I-95129 Catania, Italy*
[2] *Université de Liège, Institut de Physique B.5, Sart Tilman, B-4000 Liege 1, Belgium*

Received 8 May 1991
(Revised 26 July 1991)

Abstract: The $^3P_2$ neutron superfluidity and the $^1S_0$ proton superfluidity in neutron star matter are investigated by solving the gap equation exactly for a realistic nucleon–nucleon potential, namely the Argonne v_{14} potential. For the $^3P_2$ case, our results point to a nearly isotropic pairing function, in close analogy with the rigorous result obtained by Balian and Werthamer for $S=1$ pairing without J-dependence. The proton abundance and the $^1S_0$ proton gap are calculated and their relationship with the symmetry energy is discussed.

1. Introduction

There is presumed a realization of superfluidity in three different regions of a neutron star [1,2]). In the inner crust, the $^1S_0$ neutron superfluid pervades an array of neutron rich nuclei. In the core, the neutrons are superfluid, due to the $^3P_2$ pairing. In a region beginning in the inner crust and extending far inside the core, the protons form a superfluid owing to $^1S_0$ pairing. The main properties of these superfluids have been grossly known for a long time. Yet, there is a renewed interest in these problems [3–5]), either because of recent developments in many-body theories or because of a possible re-examination in the light of sophisticated modern two-body interactions. We are engaged in a program related to the second aspect. In a preceding paper [4]), we have recalculated the $^1S_0$ pairing properties both for neutron and nuclear matter, using standard BCS theory and Paris or Argonne v_{14} potentials. We found that these potentials yield roughly the same results, similar to those obtained with other realistic potentials, although there are significant differences as far as the boundaries of the domain of superfluidity (in density and in temperature) and the maximum value of the gap are concerned. In this paper, we pursue this program and examine the $^3P_2$ neutron pairing and the $^1S_0$ proton pairing in neutron star matter. In the future, we will calculate the effect of corrections to the pairing interaction. The results presented here are thus only indicative and should be compared to other calculations neglecting induced interactions.

The pairing in all cases ($^1S_0$, $^3P_2$ neutrons, $^1S_0$ protons) is important for the cooling of neutron stars. Besides that, $^3P_2$ neutron superfluidity might influence the coupling

between the rotational energy of the core and that of the crust. The importance of proton superfluidity for neutron star dynamics is less clear. Although the proton fluid is superconducting, it seems to have little influence on the magnetic properties of the star [2,6,7]).

The paper is organized as follows. In sect. 2, we discuss the $^3P_2$ neutron pairing, both in the so-called $|m|=2$ and $m=0$ configurations. We also discuss qualitatively more general configurations. In sect. 3, we investigate the $^1S_0$ proton pairing, taking account of the neutron background, and discuss its relationship with the symmetry energy. In sect. 4, we briefly comment on the implications of our results and present our conclusion.

2. $^3P_2$ neutron pairing

2.1. GENERAL EQUATIONS

The structure of the gap equation for anisotropic pairing is well known [8,9]). For the $^3P_2$–$^3F_2$ channel, it can be simplified, as the $^3F_2$ phase is so small that a pure $^3P_2$ wave can safely be considered [9]). The gap equation still involves five components. In general, they can be written as:

$$\Delta_m(k) = -\frac{2}{\pi}\int_0^\infty \mathrm{d}k'\, k'^2 \langle k|V(^3P_2)|k'\rangle \int \mathrm{d}\hat{k}' \sum_{m'} \frac{\Delta_{m'}(k')\,\mathrm{Tr}\{G_{m'}(\hat{k}')G_m^*(\hat{k}')\}}{2\tilde{E}(k)}, \tag{2.1}$$

where the generalized gap function is defined as

$$\Delta(k) = \sum_m \Delta_m(k) G_m(\hat{k}), \tag{2.2}$$

with

$$G_m(\hat{k}) = \sum_{m_l}\sum_{m_s} (1m_s 1m_l|2m)\, Y_1^{m_l}(\hat{k})(\tfrac{1}{2}\sigma_1\, \tfrac{1}{2}\sigma_2|1m_s). \tag{2.3}$$

The latter quantity is a matrix in the spin indices σ_1 and σ_2 of the two pairing particles. The quasi-particle energy $\tilde{E}(k)$ is given by

$$\tilde{E}(k) = [(e(k)-\mu)^2 + D^2(k)]^{1/2}, \tag{2.4}$$

where $e(k)$ is the Brueckner–Hartree–Fock single-particle energy, μ is the chemical potential and $D^2(k)$ is given by

$$D^2(k) = \tfrac{1}{2}\sum_m \sum_{m'} \Delta_m^*(k)\Delta_{m'}(k)\,\mathrm{Tr}\{G_m^*(\hat{k})G_{m'}(\hat{k})\}. \tag{2.5}$$

One can show that time-reversal invariance implies that

$$\Delta_m^*(k) = (-)^m \Delta_{-m}(k). \tag{2.6}$$

2.2. $|m|=2$ AND $m=0$ CONFIGURATIONS

As far as we know, equations (2.1) have not been solved in their full complexity. Many authors have argued [8,9]) that a simple configuration

$$\Delta(k)=\Delta_2(k)(G_2(\hat{k})+G_2^*(\hat{k})) \tag{2.7}$$

is favoured. This configuration, denoted as the $|m|=2$ configuration is consistent with requirement (2.6). In such a case, eq. (2.1) reduces to a single equation. It implies nevertheless an integration over the angles.

However, in ref. [10]) it has been argued that the $m=0$ configuration

$$\Delta(k)=\Delta_0(k)G_0(\hat{k}) \tag{2.8}$$

could be favoured energetically. We first looked at solving the gap equation for these two configurations, using the separable version [11]) of the v_{14} Argonne potential [12]) and the single-particle spectrum $e(k)$, as calculated in the frame of the first-order g-matrix Brueckner theory. The results for $\Delta_2(k_F)$ and $\Delta_0(k_F)$ at zero temperature are given in fig. 1. The dots are obtained with a fully self-consistently determined single-particle spectrum. This procedure cannot be extended beyond, say $k_F \sim 2.5\ \mathrm{fm}^{-1}$, since there are serious concerns about the convergence of the Brueckner series in this density range. We therefore first check that using a global fit of the single-particle energy spectrum with a constant effective mass formula (the resulting effective mass is given in fig. 2) did introduce only minor changes in $\Delta(k)$, and then used an extrapolation of our determined effective mass to higher densities. In practice, we use a linear extrapolation as a function of the baryon density. This procedure is consistent with the results of ref. [13]) and appears quite reasonable in view of fig. 2. The results for the gap are given by the full lines in fig. 1. We see that the gap is maximum around $k_F \sim 2.7\ \mathrm{fm}^{-1}$, i.e. at a neutron density around $\rho_B \sim 4\rho_0$. Furthermore, for all values of k_F, the $m=0$ gap is larger than that for $|m|=2$.

2.3. CONDENSATION ENERGY

We calculated the condensation energy for each configuration. Typical values are given in table 1. Systematically, the condensation energy is about the same for both configurations. This result is at variance with that obtained in ref. [10]), although the authors of this work do not give their results for the difference in the condensation energy for the two configurations. Incidentally, we notice that the approximate formula [14])

$$E_c/A=-\tfrac{3}{8}\langle\Delta^2\rangle/T_F^*, \tag{2.9}$$

where $T_F^*=\hbar^2k_F^2/2m^*$ works rather well for $m=0$, provided one uses for $\langle\Delta^2\rangle$ the angle-averaged value of the quantity $D^2(k_F)$ entering the expression of the quasi-particle energy (2.4). The same remark applies to the $|m|=2$ case (see below).

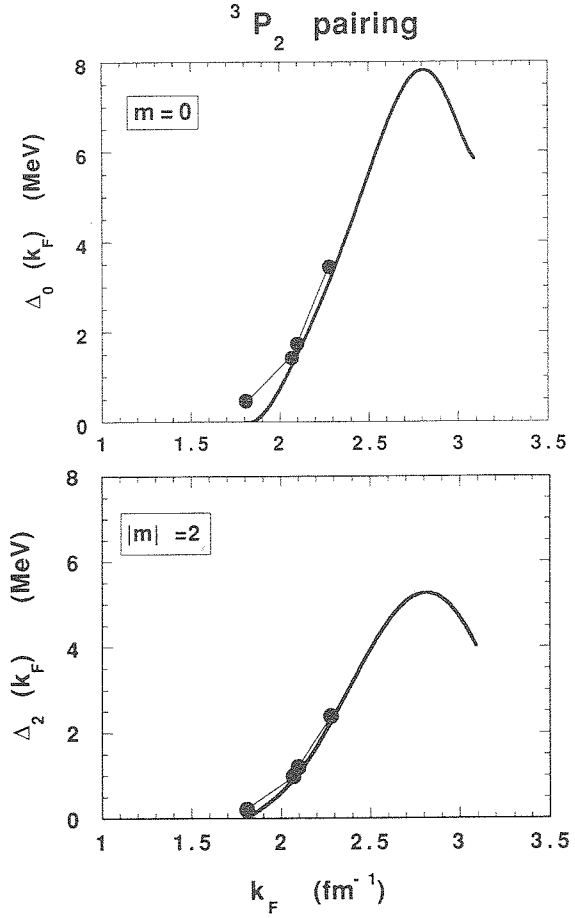

Fig. 1. Calculated value of the gap function (eq. (2.2)) at Fermi momentum in the $^3P_2$ channel for the $m=0$ and $|m|=2$ configurations. The dots correspond to a calculation with the fully self-consistent single-particle spectrum and the full curves to a constant effective mass approximation for this spectrum.

Note that the gap functions are normalized according to eqs. (2.7) and (2.8). See text for details.

2.4. DISCUSSION

All these surprisingly similar results for the condensation energy can be understood by the following considerations. We can, for instance, rewrite the $m=0$ gap equation as

$$\Delta_0(k) = -4\int_0^\infty \mathrm{d}k'\, k'^2 \langle k|V(^3P_2)|k'\rangle \int_{-1}^{+1} \mathrm{d}(\cos\theta)\, \frac{\Delta_0(k')(1+3\cos^2\theta)/8\pi}{2\tilde{E}(k',\theta)}, \tag{2.10}$$

with

$$\tilde{E}(k',\theta) = \left[(e(k')-\mu)^2 + \tfrac{1}{2}\Delta_0^2(k')\,\frac{1}{8\pi}(1+3\cos^2\theta)\right]^{1/2}. \tag{2.11}$$

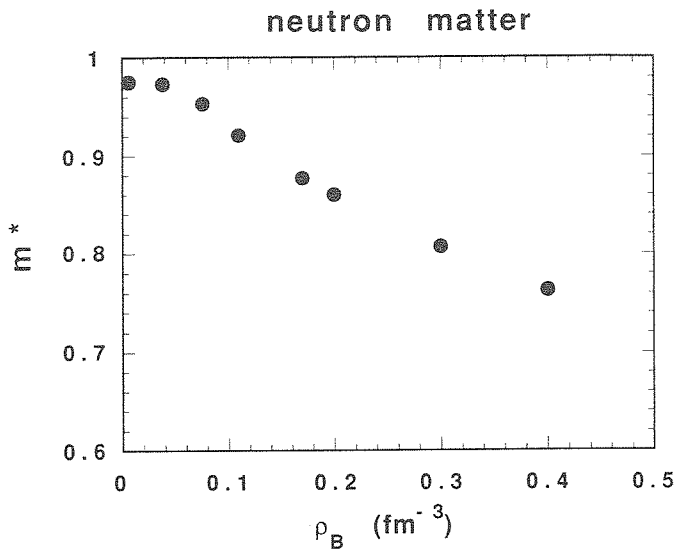

Fig. 2. Neutron effective mass in neutron matter, as a function of the baryon density, calculated in the Brueckner–Hartree–Fock approximation, with the v_{14} potential. See text for detail.

As shown in fig. 3, it turns out that the angle dependence of $\tilde{E}(k', \theta)$ is not as important as one might think at first. The solution, using the average value of the angle-dependent functions in (2.10), i.e. applying the substitution (both in the numerator of (2.10) and in expression (2.4) of $\tilde{E}(k', \theta)$)

$$\frac{1}{8\pi}(1+3\cos^2\theta) \to \frac{1}{4\pi}, \tag{2.12}$$

is rather close to the true solution, the largest discrepancy (5–10%) arising slightly above k_F. (Incidentally, we notice that the gap function vanishes at $k=0$, as it

TABLE 1

Value of the neutron gap $\Delta_m(k_F)$ (in MeV) and of the condensation energy per nucleon E_C (in keV), in the $m=0$ and $|m|=2$ configurations for various values of k_F. The last column gives the condensation energy, as calculated by eq. (2.9). See text for detail.

	$\|m\|=2$		$m=0$		
k_F (fm^{-1})	$\Delta(k_F)$ (MeV)	E_C (keV)	$\Delta(k_F)$ (MeV)	E_C (keV)	E_C (keV) eq. (2.9)
2.07	0.99	−0.18	1.42	−0.192	−0.229
2.1	1.2	−0.296	1.73	−0.299	−0.265
2.28	2.6	−1.2	3.44	−1.24	−1.028

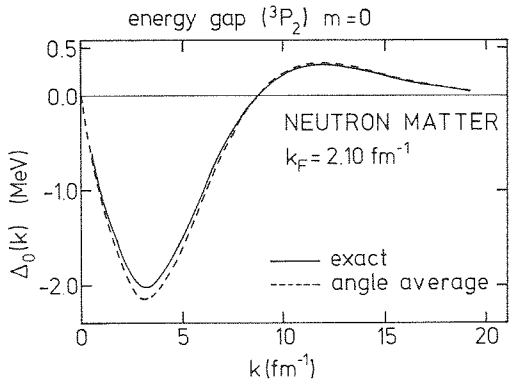

Fig. 3. Gap function $\Delta_0(k)$ in the $^3P_2$ channel and for the $m=0$ configuration. The full curve corresponds to the exact solution of the gap equation, whereas the dotted line corresponds to the solution obtained by taking angle-average quantities in eq. (2.10). See text for detail.

should be the case for $l=1$ waves). Similarly, the $|m|=2$ gap equation can be written as

$$\Delta_2(k) = -4\int_0^\infty \mathrm{d}k'\, k'^2 \langle k|V(^3P_2)|k'\rangle \int_{-1}^{+1} \mathrm{d}(\cos\theta)\, \frac{3\Delta_2(k')(1-\cos^2\theta)/8\pi}{2\tilde{E}(k',\theta)}, \tag{2.13}$$

with

$$\tilde{E}(k',\theta) = \left[(e(k')-\mu)^2 + \tfrac{1}{2}\Delta_2^2(k')\,\frac{3}{4\pi}(1-\cos^2\theta)\right]^{1/2}. \tag{2.14}$$

We also checked that using angle-averaged quantities in eq. (2.13), i.e. owing to the substitution

$$\frac{3}{4\pi}(1-\cos^2\theta) \to \frac{1}{2\pi}, \tag{2.15}$$

yields also results very close to the exact results. If the angle-dependence can be neglected, then very simple results arise:

(i) If we call $\delta_0(k)$ the solution for the uncoupled $m=0$ equation, the solution for the uncoupled $|m|=2$ equation is $\Delta_2 = \sqrt{\frac{1}{2}}\delta_0$, as one can verify by simple inspection of eqs. (2.10) and (2.13) with the substitutions (2.12) and (2.15), respectively. Our results, shown in fig. 1, are very close to this simple result.

(ii) In the same conditions, the coupled $m=0, \pm 2$ equations yield $\Delta_2 = \Delta_{-2} = \Delta_0 = \sqrt{\frac{1}{3}}\delta_0$.

(iii) The totally coupled $m=0, \pm 1, \pm 2$ equations yield $\Delta_2 = \Delta_{-2} = -i\Delta_1 = i\Delta_{-1} = \Delta_0 = \sqrt{\frac{1}{5}}\delta_0$.

(iv) In all cases (mixed or not), the condensation energy is the same as in the pure $m=0$ configuration and the quasi-particle energy is simply

$$\tilde{E}(k)=\left[(e(k)-\mu)^2+\frac{\delta_0^2(k)}{8\pi}\right]^{1/2}. \tag{2.16}$$

It seems that, in the actual situation, all the configurations are practically degenerate with respect to the condensation energy. For symmetry reasons, an isotropic (or quasi-isotropic) configuration is expected. Balian and Werthamer [15]) proved that the gap function should be isotropic for $S=1$ pairing if J-dependence is neglected. Our calculations showed that this also holds with good accuracy for the specific $^3P_2$ neutron pairing. If we examine the structure of eqs. (2.10) and (2.13), we see that the angle dependence is of small importance if the integration is practically restricted to nearly $k' \approx k_F$, since it then cancels out $(e(k)-\mu \approx 0)$. This situation is roughly controlled by the parameter $\Delta(k_F)/T_F^*$: the smaller this parameter, the narrower is the effective integration domain. Therefore the isotropy ultimately arises from a weak pairing (which gives a small $\Delta(k_F)$) combined with a large T_F^*.

2.5. TEMPERATURE DEPENDENCE

We also solved the $m=0$ and $|m|=2$ decoupled gap equations for finite temperature, i.e. introducing a factor $\tanh(\frac{1}{2}\beta\tilde{E})$ in the gap equation, where β is the inverse temperature. The results are given in fig. 4 for a typical value of k_F. One sees that the critical temperature is the same for both cases ($T_c \approx 0.4$ MeV). One

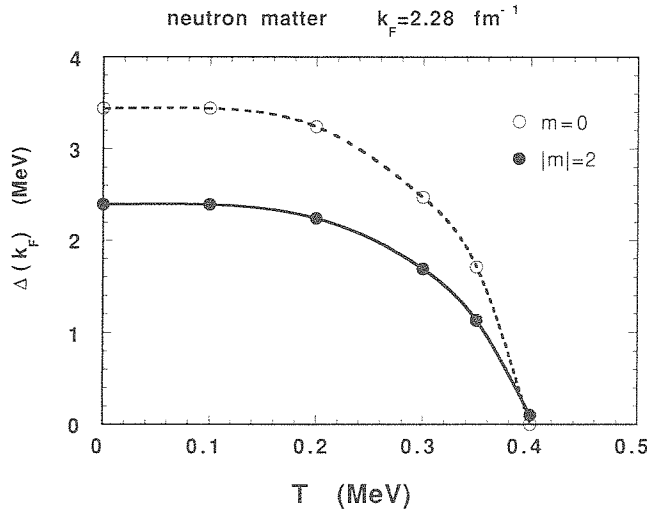

Fig. 4. Value of the gap function (in the $^3P_2$ channel) at $k=k_F$ as a function of the temperature T for $m=0$ (open dots) and $|m|=2$ (full dots) configurations. The calculation refers to neutron matter at $k_F=2.28$ fm^{-1}.

can also verify that the approximate formula [14])

$$T_c \approx 0.57\Delta(T=0) \tag{2.17}$$

gives a quite reasonable approximation to the exact value of T_c, provided one uses for $\Delta(T=0)$, the square root of the angle-averaged value of $D^2(k_F)$. One has $\langle D^2(k_F)\rangle = \Delta_0^2/8\pi$ for $m=0$ and $\langle D^2(k_F)\rangle = \Delta_2^2/4\pi$ for $|m|=2$. Numerically $\Delta_0 \simeq \Delta_2\sqrt{2}$, which yields about the same value of $\langle D^2(k_F)\rangle$ in both cases. This is also the reason why formula (2.9) yields the same result for $m=0$ and $|m|=2$ cases.

3. $^1S_0$ proton superfluidity

3.1. THE ABUNDANCE OF THE PROTON CONTAMINANT

We first determine the proton abundance in uniform neutron star matter for the interaction we have chosen. For this purpose, we minimize the energy per baryon of uniform neutron star matter, composed of neutrons, protons and electrons at baryon density ρ_B, $W(\rho_B, x)$ with respect to the proton abundance $x = Z/A$. The matter being electrically neutral, x is also the ratio of electron number density to baryon number density. If we assume that the electron energy can be approximated by the relativistic gas expression and if the various components have uniform densities, the energy per baryon can be written as

$$W(\rho_B, x) = W_B(\rho_B, x) + \frac{(m_e c^2)^4}{\pi^2(\hbar c)^3 \rho_B} \times [\tfrac{1}{4}x_F(x_F^2+1)^{3/2} - \tfrac{1}{8}x_F(x_F^2+1)^{1/2} - \tfrac{1}{8}\ln(x_F + \sqrt{x_F^2+1})], \tag{3.1}$$

where the first term is the baryon average energy and where

$$x_F = (2x)^{1/3}\frac{\hbar k_F}{m_e c}, \tag{3.2}$$

$$\rho_B = \frac{2}{3\pi^2}k_F^3. \tag{3.3}$$

The quantity k_F is the Fermi momentum the matter would have if it was symmetric ($N=Z$). The neutron and proton (as well as electron) Fermi momenta are respectively given by

$$k_F^n = [2(1-x)]^{1/3}k_F, \qquad k_F^p = k_F^e = (2x)^{1/3}k_F. \tag{3.4}$$

For W_B, we used the first-order g-matrix Brueckner expression calculated with the v_{14} Argonne potential. It can then be written as

$$W_B(\rho_B, x) = \frac{E_0}{A}(\rho_B) + (1-2x)^2 E_s(\rho_B) + M_n c^2(1-x) + M_p c^2 x, \tag{3.5}$$

where the first term is the binding energy per nucleon for symmetric nuclear matter, and where E_s (ρ_B) is the so-called symmetry energy. The quadratic dependence upon $\beta = (N-Z)/A = 1-2x$ is not dictated from first principles. However, it follows from the numerical results with a very good accuracy, even for β close to one $(x \ll 1)$, as described by the work of ref. [16]). The proton abundance x is then given by the solution of the equation:

$$\frac{dW}{dx}(\rho_B, x) = -4(1-2x)E_s(\rho_B) - (M_n - M_p)c^2 + m_e c^2\sqrt{(2x)^{2/3}(\hbar k_F/m_e c)^2 + 1} = 0 . \tag{3.6}$$

Its numerical value is given in fig. 5, along with previous results from Nemeth and Sprung [17]) and from Chao *et al.* [18]). The origin of the rather large differences lies basically in the strong dependence upon the symmetry energy, as it appears clearly when both the limit of small x in W_B (neglect of x in the first term of (3.6)) and the ultrarelativistic expression for the electron energy (neglect of unity under the square root sign) are employed. One then simply obtains

$$x \simeq \frac{1}{2}\left(\frac{4E_s}{\hbar c k_F}\right)^3 . \tag{3.7}$$

It is interesting to note that the domain of k_F (from ~ 0.8 to $\sim 2\,\mathrm{fm}^{-1}$) where we made our numerical investigations, the ultrarelativistic approximation is quite good: see the difference between the open dots and the lozenges in fig. 6 (the difference between the full calculation and its ultrarelativistic approximation are not even distinguishable on the scale of the figure). The small x approximation, which amounts

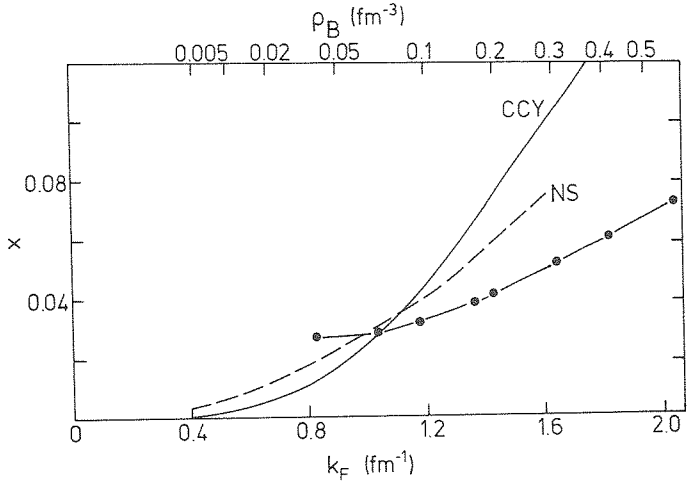

Fig. 5. Proton fraction x of neutron star matter as a function of the baryon density ρ_B (upper scale) or of the Fermi momentum k_F (lower scale). The results of this work (full dots) are compared with those of ref. [17]) (NS) and of ref. [18]) (CCY).

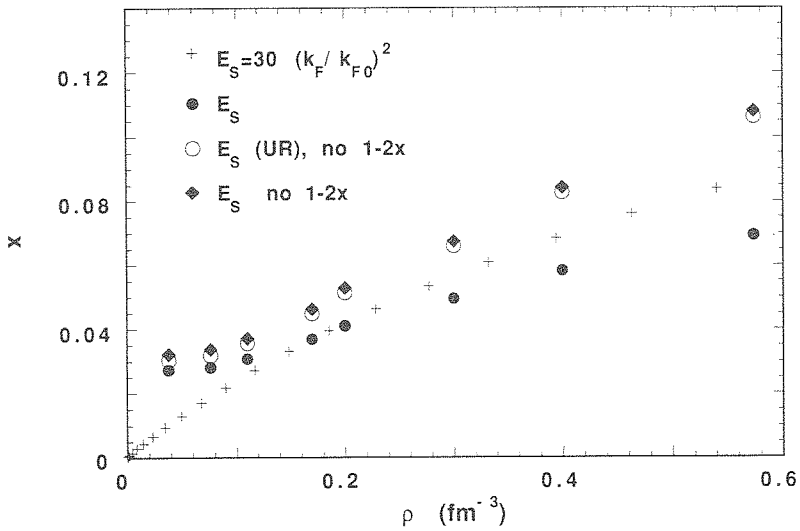

Fig. 6. Proton fraction x of neutron star matter in various calculations: exact calculation with the v_{14} potential (full dots); calculation using a simple parametrization (eq. (3.8)) of the symmetry energy (plusses); calculation with v_{14} potential, but using the ultrarelativistic expression for the free electron gas and neglecting the factor $(1-2x)$ in expression (3.6) (open dots); calculation neglecting this factor only (lozenges).

to neglect the factor $1-2x$ in the first term of eq. (3.6) is less accurate (difference between the full dots and the lozenges).

In our calculation, the behaviour of x at the lowest values of k_F investigated is different from that of refs. [17,18]) and seems to indicate a non-zero value of x at large dilution. This seems even more apparent in fig. 6. Although this issue is of no important consequence for neutron stars, it is nevertheless interesting to discuss. Indeed, in fig. 6, we also show the result obtained using a simple parametrization of E_s, namely

$$E_s = 30\,(k_F/k_{F_0})^2\ \text{MeV}\,, \tag{3.8}$$

where k_{F_0} is normal nuclear matter Fermi momentum ($=1.36\ \text{fm}^{-1}$). Expression (3.8), proposed in ref. [19]), has been obtained by fitting numerical results for nearly symmetrical matter in the ρ_0 range, where it agrees more or less with the results of ref. [15]) used here. For $\sim 0.2 < \rho_B < 1.0\ \text{fm}^{-3}$, the value of E_s, calculated in ref. [16]) and used in our calculations, is smaller than that given by eq. (3.8). For $0.03 < \rho_B \lesssim 0.2\ \text{fm}^{-3}$, the converse is true. This explains our rather large value of x in this density range. Note that at still smaller density, $E_s\ (\rho_B)$ will eventually be given by the Fermi gas approximation only, i.e. $E_s\ (\rho_B) \simeq 6k_F^2$, when E_s is expressed in MeV and k_F in fm^{-1}. This will give (see eq. (3.7)) a decreasing value of x. But this regime sets in around $\rho \lesssim 0.01\ \text{fm}^{-3}$. Ultimately, when the density is smaller than $10^{-7}\ \text{fm}^{-3}$, the electron gas will be nonrelativistic, only the mass terms are important in eq. (3.6), and x tends to unity.

The above discussion about the low-density behaviour pertains to uniform matter only and aims to assess the adequacy of our numerical results. It is somewhat academic since at $\rho_B \lesssim 0.8\,\rho_0$, where neutron star matter is expected to nucleate.

3.2. PROTON SINGLE-PARTICLE ENERGY

The single-particle spectrum has been calculated self-consistently and *simultaneously* for protons and neutrons. The results for the average field are given in fig. 7 for $\rho_B = 0.17\,\mathrm{fm}^{-3}$. The corresponding Fermi momentum for protons k_F^p is $0.571\,\mathrm{fm}^{-1}$. The average field is split into contributions due to the interaction with each kind of nucleons

$$U_p = U_p^{(pp)} + U_p^{(np)} . \tag{3.9}$$

The value of U_p is compared with the average field U_p^0 in pure proton matter (without Coulomb forces) with the same k_F^p. The main effect is a dramatic increase of U_p due to the interaction with the neutron background. The quantity $U_p^{(np)}$ is roughly twice as large as the average field felt by a neutron in pure neutron matter

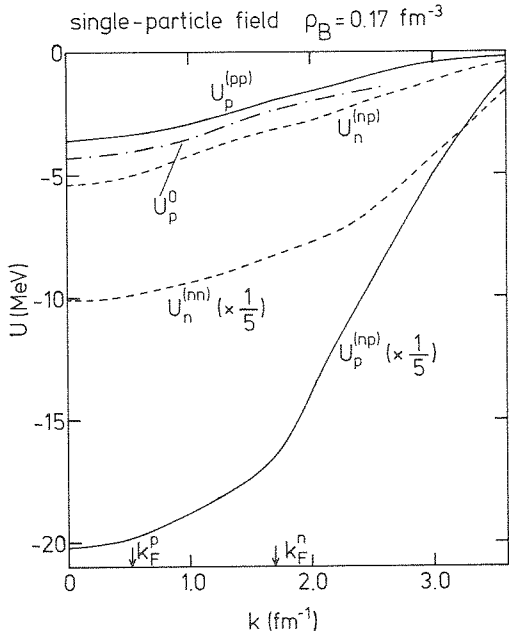

Fig. 7. Single-particle field in neutron star matter at baryon density $\rho_B = 0.17\,\mathrm{fm}^{-3}$ as a function of momentum k, calculated in Brueckner–Hartree–Fock approximation and with v_{14} potential. The quantity $U_n^{(nn)}$ (resp. $U_p^{(pp)}$) is the average potential felt by a neutron (resp. proton) due to its interaction with the other neutrons (resp. protons). The quantity $U_n^{(np)}$ (res. $U_p^{(np)}$) is the average potential felt by a neutron (resp. proton) due to neutron–proton interaction. The quantity U_p^0 is the proton single-particle potential in pure proton matter with the same proton Fermi momentum. The values of the proton Fermi momentum k_F^p and of the neutron Fermi momentum k_F^n are indicated by the arrows.

U_n^0 with the same k_F^n (see ref. [20])), which is about the same as that felt by a neutron in the neutron star matter under consideration. The big difference between $U_p^{(np)}$ and U_n^0 is due to the relaxation of the Pauli operator for the np pair when one calculates in first-order g-matrix and, more importantly, to the allowance of $T=0$ channels for this pair. The factor one-half between U_n^0 and $U_p^{(np)}$ does not come simply when inspecting the mathematical formula, but is consistent with the quadratic dependence of $W_B(\rho_B, x)$ upon x and the numerical values of the average fields in nuclear matter and in neutron matter. Indeed, as indicated in ref. [20]), for a given baryon density, if W_B is quadratic in x, the following form of the mean field is expected:

$$U(k, \tau, x) = U_0(k) - \tfrac{1}{4}\tau(1-2x)U_1(k)\,, \tag{3.10}$$

where $\tau = +1$ for protons and -1 for neutrons. The quantity U_0 is the mean field in nuclear matter. For $\rho = \rho_0$ and $k \simeq 0$, $U_0 \simeq -80$ MeV. The quantity $U_1 \simeq 120$ MeV for $k \simeq 0$. Therefore, for $x \ll 1$, $U_n \simeq 50$ MeV, whereas $U_p \simeq 110$ MeV.

Note also the small reduction of $U_p^{(pp)}$, compared to U_p^0, due to the nonlinearity coming from the simultaneous self-consistency requirements in defining the nucleon spectrum and solving the g-matrix equation for pp, nn and np pairs.

As far as the gap properties are concerned, the strong enhancement of the average proton potential is not as important as it might appear at first sight. What matters indeed is the possible modification of its curvature (with k). The latter can conveniently be characterized by a constant effective mass approximation for U_p^{total} (eq. (3.9)). The extracted effective mass m^* is given in fig. 8, as a function of the total baryon density ρ_B. The proton effective mass first decreases due to the attractive interaction with the denser and denser neutron background, and afterward levels off around 0.7 for $\rho_B \simeq 0.2\,\text{fm}^{-3}$. We also make a comparison with the neutron effective mass for pure neutron matter. The latter is substantially larger, as indicated by fig. 7. We stress that all the calculations of the gap presented below have been carried out with the true single-particle spectrum and not the effective mass approximation. Incidentally, we remark that the effective masses indicated in fig. 8 correspond to the local (in k) effective mass close to the Fermi surface. The global effective mass, i.e. the mass parameter extracted from a global fit of $e(k)$, is larger. This partly explains the difference between the results given in fig. 8 for the neutron effective mass and those of ref. [20]) (see fig. 7 of this reference), which, however, uses another interaction, namely the Paris potential.

3.3. RESULTS FOR THE $^1S_0$ PROTON PAIRING

Our results for the $^1S_0$ pairing using self-consistently calculated single-particle spectrum and the v_{14} Argonne potential are given in fig. 9. The same results are also plotted in fig. 10, as a function of the baryon density, corresponding to the proton fraction at the equilibrium with respect to weak interactions (beta decay). There is

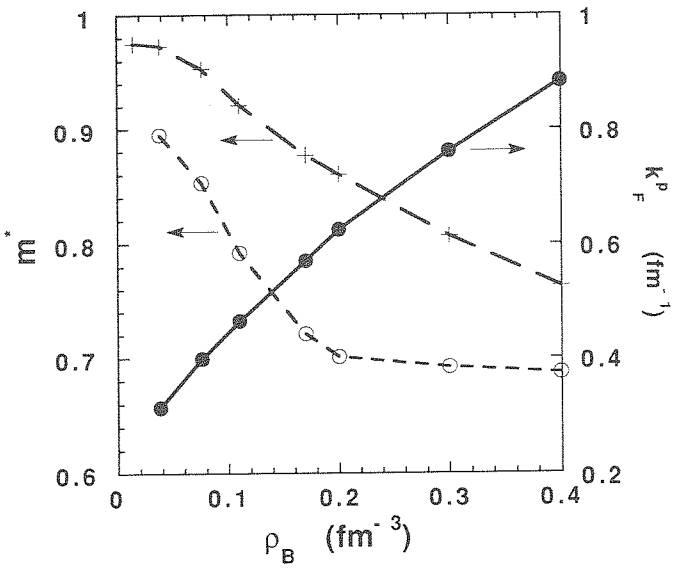

Fig. 8. Neutron (crosses) and proton (open dots) effective mass (in units of nucleon mass) in neutron star matter, as a function of the latter's baryon density ρ_B. The full dots give the variation of the proton Fermi momentum (scale on the right side).

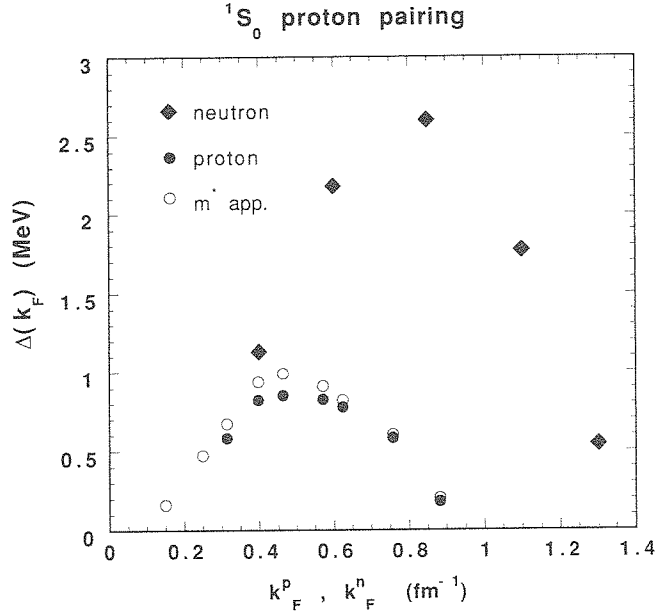

Fig. 9. Calculated value of the gap function at the proton Fermi momentum for proton $^1S_0$ pairing in neutron star matter, as a function of the Fermi momentum (full dots). The open dots refer to the same quantity, but calculated with a constant effective mass approximation. For the sake of comparison, the neutron gap in neutron matter (squares) is shown.

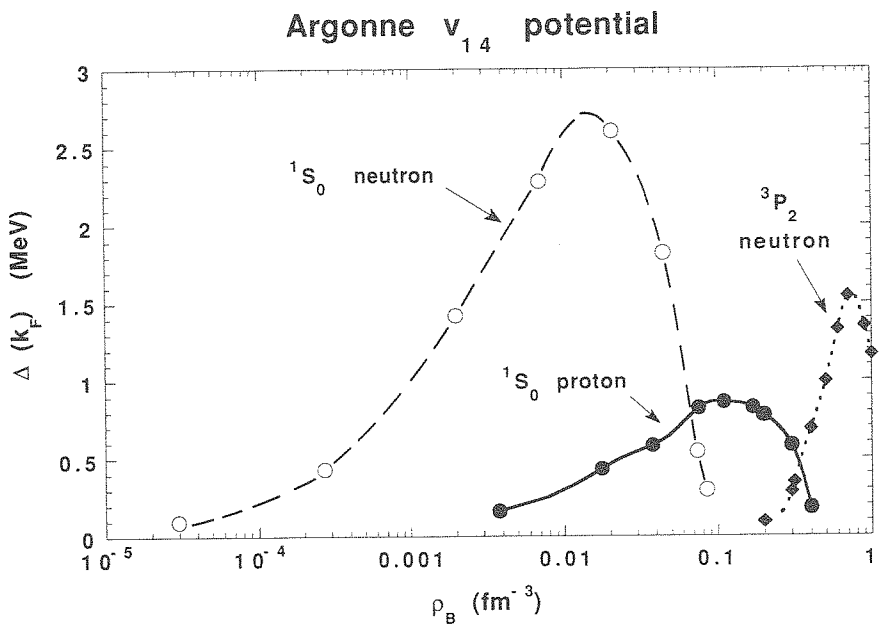

Fig. 10. Gap for the various kinds of superfluidity in neutron star matter at baryon density ρ_B. See text for detail.

a maximum value of the gap of ~0.8 MeV at $k_F^p \approx 0.4\,\mathrm{fm}^{-1}$. This is roughly a factor of 3 smaller than the maximum value of the $^1S_0$ neutron gap in neutron matter. Furthermore the gap domain ends at a smaller Fermi momentum (~0.9 fm^{-1} against ~1.4 fm^{-1} in the latter case). The main reason comes from the smaller proton effective mass, which reduces the gap, as simple approximations like eq. (5.2) in ref. [4]) indicate.

The open points in fig. 9 give the value of the gap when the single-particle spectrum is approximated by a constant effective mass formula around the Fermi momentum. One can see that the effect of the true single-particle spectrum or, equivalently, of the non-constant effective mass is not negligible.

3.4. THREE-BODY FORCES

In this section, we have considered the binding energy of neutron star matter using two-body forces only. It is well known that this approach does not yield a satisfactory binding of symmetric matter. However, it is clear from our discussion that the proton pairing properties does depend basically upon the proton effective mass, as the approximate popular formula for $^1S_0$ pairing indicates:

$$\Delta(k_F) = \xi \frac{\hbar k_F^2}{2m^*} \exp\left[4\pi^2 \frac{\hbar^2 k^2}{2m^* \langle k_F | V(^1S_0) | k_F \rangle k_F^3}\right] \qquad (3.11)$$

(ξ is a numerical factor of the order of a few units). As indicated by fig. 7, the effective mass depends moderately on the proton abundance (the proton fraction is roughly responsible for the $U_p^{(pp)}$ part of the proton average potential), which in turn depends mainly upon symmetry energy (see eq. (3.7)). Both the effective mass and the symmetry energy are linked with relative variations of the binding energy and not so much on its absolute value. Therefore, it is expected that they depend mainly on two-body forces and weakly on three-body forces, that, for part of them, are introduced phenomenologically to obtain good saturation properties in nuclear matter. This statement is certainly valid for the pairing itself. The proton abundance seems to be more sensitive to the importance of three-body forces, as demonstrated in ref. [21]), especially for ρ_B larger than $\sim 1.5\,\rho_0$. The issue about the proton abundance value for larger baryon density is far from being settled, since the precise knowledge of the three-body force is not under complete control. For illustrative purpose, we refer to the results of ref. [16]), where it is shown that the introduction of the three-body forces quoted in ref. [20]) does not practically change our proton abundance value for $\rho \simeq 0.11$–$0.4\ \mathrm{fm}^{-3}$. For smaller densities, it is lowered. Furthermore, in the same range, our values are close to that obtained in ref. [21]) with what is called UVII three-body interactions.

4. Discussion and conclusion

In ref. [4]) and in this paper, we have calculated, using a realistic potential, namely Argonne v_{14} potential, and standard BCS theory, the pairing properties of the three realizations of superfluidity in neutron star matter. They are summarized in fig. 10. For the $^3P_2$ pairing, we have plotted the quantity $\Delta_0(k_F)/\sqrt{8\pi}$, or equivalently in our calculation, $\Delta_2(k_F)/\sqrt{4\pi}$, which is the quantity entering the expression of the quasi-particle energy (see eq. (2.16)). This procedure allows a meaningful comparison with the gap function for the $^1S_0$ pairing, as the convention in the latter case is to define the gap function such that there is no numerical factor in the expression of the quasi-particle energy.

Although our results are qualitatively similar to those of previous investigations, there are nevertheless substantial differences. In our case, there is a clear separation between the $^1S_0$ and $^3P_2$ neutron superfluidity domains. On the other hand, we predict a stronger $^3P_2$ pairing than in refs. [1,10,22]) and about the same as in the work by Tamagaki [9]), who however used a very crude interaction. Furthermore, our calculations show a proton superfluidity which extends well inside the $^1S_0$ neutron superfluidity domain, which is at variance with previous calculations [17,18]).

We also worked out other results. First, we have shown that, for the $^3P_2$ neutron superfluidity, the gap function is practically isotropic, which is at variance with previous results [10,21]). Second, we have shown that the proton fraction would probably remain more important (around 3%) than previously indicated, for smaller baryon density (see fig. 6). This is linked with a stronger symmetry energy in this

density range. Finally, we presented and discussed fully self-consistent neutron and proton effective masses for neutron star matter.

Concerning the $^3P_2$ neutron pairing and $^1S_0$ proton pairing, our results can be considered as the only ones which have been obtained with a correct (self-consistent) single-particle spectrum and a modern nucleon–nucleon potential. We recall that they are obtained in the frame of the standard BCS theory, using the first-order (bare) particle–particle interaction as the pairing interaction. As we already discussed in our previous work [4]), the results are not expected to depend upon the potential, provided the latter reproduces phase shifts correctly. However, for the proton superfluidity, the full calculation depends in addition critically upon the symmetry energy predicted by this potential. Indeed, the gap depends sensitively upon the proton effective mass, which in turn depends moderately upon the symmetry energy.

As far as neutron star physics is concerned, our results have some (limited) importance. First, the large proton gap may limit more than previously believed [6]) the penetration of the proton superfluid by magnetic fields. Second, the strong $^3P_2$ neutron pairing, found in our calculation, may modify the previous estimates of the cooling rate of neutron stars. Furthermore, it could also influence the coupling between the crust and core superfluids. However, it is now increasingly considered [2,23]) that this coupling occurs primarily through the pinning of vortex lines in the neutron superfluid of the crust by the nuclei of the crust. The crucial parameters in the coupling would then depend upon the $^1S_0$ neutron pairing only.

We keep in mind that, even if our calculation is one of the more detailed ones, it should be improved before definite conclusions about neutron star physics can be drawn. First, the approach of the $^3P_2$ pairing in very dense matter with nucleon–nucleon potentials is certainly one of the more questionable features. Second, and more importantly, the whole problem of superfluidity in neutron star matter should be studied with a more elaborate particle–particle effective interaction [24]). [It is our purpose to introduce in a future work the so-called polarization term [24]) in the pairing interaction.] It is already clear from the works of refs. [3,25]) that the so-called induced interaction in the $^1S_0$ channel may have dramatic consequences on the value of the pairing gap as well as on the extension of the superfluidity domain in k_F. In ref. [3]), the induced interaction is introduced in first order. It gives a strong reduction of the pairing. In ref. [25]), it is shown that higher-order contributions somehow counterbalance this reduction. The resulting gap may, however, be a factor 2 smaller than its value without induced interactions, especially at low density. According to ref. [25]), the maximum value of the $^1S_0$ neutron gap would be decreased from 2.7 MeV (fig. 10) to ~1.3 MeV. On the other hand, it seems that the gap may be increased at higher densities.

References

1) G. Baym and C.J. Pethick, Ann. Rev. Nucl. Sci. **25** (1975) 27
2) D. Pines and M.A. Alpar, Nature **316** (1985) 27

3) J.H.C. Chen, J.W. Clark, E. Krotscheck and R.A. Smith, Nucl. Phys. **A451** (1986) 509
4) M. Baldo, J. Cugnon, A. Lejeune and U. Lombardo, Nucl. Phys. **A515** (1990) 409
5) B.E. Vonderfecht, C.C. Gearhart and W.H. Dickhoff, Phys. Lett. **B253** (1991) 1
6) G. Baym, C.J. Pethick and D. Pines, Nature **224** (1969) 673
7) D. Pines, J. de Phys. **C2** (1980) 111
8) P.W. Anderson and P. Morel, Phys. Rev. **C123** (1961) 1911
9) R. Tamagaki, Prog. Theor. Phys. **44** (1970) 905
10) M. Hoffberg, A.E. Glassgold, R.W. Richardson and M. Ruderman, Phys. Rev. Lett. **24** (1970) 775
11) M. Baldo and L.S. Ferreira, Phys. Lett. **B255** (1991) 477
12) I.E. Lagaris and V.R. Pandharipande, Nucl. Phys. **A359** (1981) 331
13) B. Friedman and V.R. Pandharipande, Nucl. Phys. **A361** (1981) 502
14) E.M. Lifshitz and L.P. Pitaevskii, Statistical physics (Pergamon, Oxford, 1980) p. 159
15) R. Balian and R. Werthamer, Phys. Rev. **131** (1963) 1553
16) I. Bombaci and U. Lombardo, to be published
17) J. Nemeth and D.W.L. Sprung, Phys. Rev. **176** (1968) 1496
18) N.C. Chao, J.W. Clark and C.H. Yang, Nucl. Phys. **A179** (1972) 320
19) P.J. Siemens, Nucl. Phys. **A141** (1970) 225
20) J. Cugnon, P. Deneye and A. Lejeune, Z. Phys. **A328** (1987) 409
21) R.B. Wiringa, V. Fiks and A. Fabrocini, Phys. Rev. **C38** (1988) 1010
22) T. Takatsuka, Prog. Theor. Phys. **50** (1973) 1755
23) D. Pines, J. Shaham, M.A. Alpar and P.W. Anderson, Prog. Theor. Phys. Suppl. **69** (1980) 376
24) A.B. Migdal, Theory of finite Fermi systems and applications to atomic nuclei (Wiley, New York, 1967)
25) T.L. Ainsworth, J. Wambach and D. Pines, Phys. Lett. **222** (1989) 173